Electronic Research Archive

https://www.aimspress.com/journal/era

ERA, 34(4): 2261–2278.
DOI: 10.3934/era.2026102
Received: 10 January 2026
Revised: 23 February 2026
Accepted: 05 March 2026
Published: 12 March 2026

Research article

Systematic comparison and optimization of parameter estimation methods for stochastic gene expression kinetics

Liang Chen[1,2], **Ying Sheng**[1,2,*], **Zhihui Xie**[2,*] **and Feng Jiao**[1,2,*]

[1] Guangzhou Center for Applied Mathematics, Guangzhou University, Guangzhou 510006, China
[2] College of Mathematics and Information Sciences, Guangzhou University, Guangzhou 510006, China

* **Correspondence:** Email: shengy7721@163.com, zhihuixie@gzhu.edu.cn, jiaof@gzhu.edu.cn.

Abstract: Accurately estimating kinetic parameters of stochastic gene expression is a key challenge in quantitative single-cell transcriptomics. Building on the strengths of traditional methods, such as the method of moments and maximum likelihood estimation (MLE), we propose a novel framework: moment-reduced MLE (MR-MLE). We combined these three parameter estimation methods with four steady-state mRNA distribution computation strategies (exact distribution expression, Laplace approximation, finite state projection (FSP), and Gauss–Jacobi quadrature) to form nine distinct inference methods. These methods were systematically compared on both synthetic and real experimental data across two core dimensions: computational efficiency and parameter estimation accuracy. Results show that the Laplace approximation yields unreliable parameter estimates; the method of moments is computationally efficient but suffers from small-sample bias; the exact distribution solution is the least computationally efficient; and the FSP method exhibits fluctuating efficiency with varying gene expression levels. Notably, MR-MLE integrated with Gauss–Jacobi quadrature achieves the optimal balance between computational speed and inference robustness. Thus, we recommend this method as the preferred choice for fitting experimental data, providing a reliable and efficient computational solution for large-scale single-cell gene expression data analysis.

Keywords: stochastic gene expression; parameter estimation method; steady-state distribution; computational efficiency; estimation accuracy

1. Introduction

Gene expression in individual cells is an inherently stochastic process due to small copy numbers of biochemical molecules and probabilistic collisions between them [1]. Live-cell imaging approaches allow a direct visualization of stochastic bursts of gene expression in living cells [2,3]. The stochasticity

of gene expression is a fundamental source of single-cell heterogeneity, and its dynamic behavior can be quantitatively characterized using mathematical models. The classical telegraph model has become the standard modeling framework for describing mRNA expression dynamics due to its ability to capture the bursting behavior of gene transcription [4–11]. By the model, one can obtain estimates of the rates of the underlying gene expression processes, thereby revealing the kinetic mechanisms of gene transcriptional regulation and providing a powerful theoretical tool for understanding regulatory principles in genetic engineering [12, 13], cell fate determination [14, 15], and therapeutic targets of disease [16, 17].

With the rapid advancement of single-cell sequencing technologies, massive and high-dimensional single-cell transcriptomic data have become commonplace [3, 18–20]. This development presents unprecedented opportunities for inferring gene expression kinetic parameters at a systems scale while also posing significant challenges to the computational scalability of parameter estimation methods. Currently, the most commonly used parameter inference methods include the method of moments [8], maximum likelihood estimation (MLE) [21], and Bayesian methods. However, the literature [22] indicates that the computational efficiency of Bayesian methods is much lower than that of MLE, so Bayesian methods are not considered for the time being. The method of moments infers parameters by matching sample moments with their theoretical counterparts, which yields unbiased estimates but often exhibits limited statistical efficiency. In contrast, MLE is theoretically asymptotically optimal, yet it incurs high computational complexity and can become unstable when data are limited or the model is misspecified.

To address these limitations, we propose a novel parameter estimation approach: the moment-reduced maximum likelihood estimation (MR-MLE). This approach is inspired by the conceptual bridge between moment matching and likelihood optimization [21]. From a statistical perspective, MR-MLE can be regarded as a specific implementation of the profile likelihood method. However, unlike traditional profile likelihood, which searches the full parameter space at a high computational cost, MR-MLE incorporates moment constraints to substantially reduce the parameter dimension and improve efficiency [9, 21]. Specifically, the method first reduces the parameter dimensionality by matching the first two theoretical moments with their sample counterparts, and subsequently applies maximum likelihood estimation within the constrained parameter subspace. This strategy thereby combines the computational efficiency of moment matching with the statistical accuracy of likelihood-based inference.

Both MLE and MR-MLE methods rely on the efficient computation of the steady-state distribution P_m, where P_m denotes the probability of having m mRNA molecules in an individual cell. At present, P_m can be expressed analytically in terms of confluent hypergeometric functions [23, 24]. However, due to its computational complexity and numerical challenges, numerous studies have proposed approximate methods for evaluating P_m. Widely used approaches include the Laplace approximation [25], the finite state projection method (FSP) [26], and the Gauss–Jacobi quadrature method [11, 27], each offering a distinct balance between accuracy and computational efficiency. In the practical context of large-scale single-cell data fitting, how to systematically evaluate and select the optimal combination strategy that balances computational efficiency and parameter estimation accuracy remains an unresolved open question.

To this end, this paper adopts the telegraph model as a unified theoretical framework to evaluate nine parameter estimation methods using both synthetic and experimental data from two

key perspectives: computational efficiency and parameter estimation accuracy. The methods considered include the method of moments, maximum likelihood estimation with the exact confluent hypergeometric solution (MLE Exact), maximum likelihood estimation with Laplace approximation (MLE Laplace), maximum likelihood estimation with the finite state projection method (MLE FSP), maximum likelihood estimation with Gauss–Jacobi quadrature (MLE G-J), moment-reduced maximum likelihood estimation with the exact confluent hypergeometric solution (MR-MLE Exact), moment-reduced maximum likelihood estimation with Laplace approximation (MR-MLE Laplace), moment-reduced maximum likelihood estimation with the finite state projection method (MR-MLE FSP), and moment-reduced maximum likelihood estimation with Gauss–Jacobi quadrature (MR-MLE G-J). In the evaluation design, this study first generates synthetic data of varying sample sizes via stochastic simulation, systematically tests the theoretical performance of each method under controlled conditions, and thereby establishes a reference benchmark for the analysis of real experimental data. Meanwhile, considering complex characteristics such as small-sample bias and extreme expression values inherent in real data, relying solely on synthetic data is insufficient to fully reflect the applicability of the methods under practical conditions. To this end, this study further incorporates real small-sample experimental data to systematically evaluate the performance and limitations of each method in practical scenarios. By integrating the analysis of synthetic data and real data, this research aims to provide a basis for method selection that achieves the optimal trade-off between efficiency and reliability for the analysis of large-scale single-cell gene expression data.

2. Materials and methods

2.1. The telegraph model

In the telegraph model, the gene is assumed to randomly switch between *off* and *on* states with activation rate k_{on} and inactivation rate k_{off}. mRNA molecules are synthesized with rate k_{b} only when the gene is *on* and are degraded with rate k_{d} either mRNA degradation or due to dilution during cell division [23, 28, 29]. In what follows, without loss of generality, we set $k_{\text{d}} = 1$, because the time can always be renormalized by the decay rate k_{d} [9, 30]. We formulate the telegraph model in mathematical terms:

$$\text{gene off} \xrightarrow{k_{\text{on}}} \text{gene on}, \quad \text{gene on} \xrightarrow{k_{\text{off}}} \text{gene off}, \quad \text{gene on} \xrightarrow{k_{\text{b}}} \text{gene on} + \text{mRNA}, \quad \text{mRNA} \xrightarrow{k_{\text{d}}} \varnothing.$$

The microstate of the gene can be represented by an ordered pair (i, m), where i is the gene state with $i = 0, 1$ corresponding to the inactive and active states, respectively, and m is the mRNA number. Let $P_{i,m}(t)$ denote the probability of having m mRNA molecules in an individual cell at time t when the gene is in state i. Then the stochastic gene expression dynamics can be described by the Markov jump process. The evolution of the Markovian dynamics is governed by the chemical master equations (CMEs):

$$\begin{cases} \dot{P}_{0,m}(t) = (m+1)P_{0,m+1}(t) + k_{\text{off}}P_{1,m}(t) - (m + k_{\text{on}})P_{0,m}(t), \\ \dot{P}_{1,m}(t) = k_{\text{b}}P_{1,m-1}(t) + (m+1)P_{1,m+1}(t) + k_{\text{off}}P_{0,m}(t) - (k_{\text{b}} + m + k_{\text{off}})P_{1,m}(t), \end{cases} \tag{2.1}$$

where $P_{1,-1}(t) = 0$.

To proceed, let $P_m(t) = P_{0,m}(t) + P_{1,m}(t)$ denote the probability of having m mRNA molecules at time t, and let $P_m = \lim_{t\to\infty} P_m(t)$ to represent the steady-state mRNA distribution. In steady state, the

CMEs given in Eq (2.1) can be solved exactly, and the steady-state distribution of protein numbers is given by [24, 30]

$$P_m = \frac{k_b^m}{m!} \cdot \frac{\Gamma(k_{on} + k_{off})\Gamma(k_{on} + m)}{\Gamma(k_{on})\Gamma(k_{on} + k_{off} + m)} \, {}_1F_1\left(k_{on} + m, k_{on} + k_{off} + m, -k_b\right), \tag{2.2}$$

where $\Gamma(\cdot)$ is the gamma function, and ${}_1F_1\left(k_{on} + m, k_{on} + k_{off} + m, -k_b\right)$ is Kummer's confluent hypergeometric function.

2.2. Parameter inference methods

2.2.1. Method of moments

For the telegraph model, its kinetic properties are entirely determined by three parameters, k_{on}, k_{off}, and k_b. While the parameters of this model can not be directly measured, they must be estimated based on a probability distribution derived from experimental data. The method of moments is to match the first three moments to their empirical values [30]. The analytical expression for the exponential moments e_n can be derived from the chemical master Eq (2.1) [30]:

$$e_n = \mathbb{E}\left[m(m-1)\cdots(m-n+1)\right] = \frac{c(c+b)\cdots(c+b(n-1))}{(a-1)a\cdots(a+n-2)},$$

where $\mathbb{E}$ denotes the mathematical expection, and $a = k_{on} + k_{off} + 1$, $b = k_b$, $c = k_{on}k_b$. Let r_1, r_2, and r_3 be the successive ratios of the first exponential moments:

$$r_1 = e_1 = \frac{k_{on}}{k_{on} + k_{off}} \cdot k_b, \quad r_2 = \frac{e_2}{e_1} = \frac{k_{on} + 1}{k_{on} + k_{off} + 1} \cdot k_b, \quad r_3 = \frac{e_3}{e_2} = \frac{k_{on} + 2}{k_{on} + k_{off} + 2} \cdot k_b.$$

From these relations, the kinetic parameters can be obtained by solving the system algebraically:

$$k_{on} = \frac{2r_1(r_3 - r_2)}{r_1r_2 - 2r_1r_3 + r_2r_3}, \quad k_{off} = \frac{2(r_2 - r_1)(r_1 - r_3)(r_3 - r_2)}{(r_1r_2 - 2r_1r_3 + r_2r_3)(r_1 - 2r_2 + r_3)}, \quad k_b = \frac{-r_1r_2 + 2r_1r_3 - r_2r_3}{r_1 - 2r_2 + r_3}. \tag{2.3}$$

In practice, the sample estimates of the first three exponential moments are computed from the observed mRNA distribution P_m as:

$$\hat{e}_1 = \sum_{m=0}^{M} mP_m, \quad \hat{e}_2 = \sum_{m=0}^{M} m(m-1)P_m, \quad \hat{e}_3 = \sum_{m=0}^{M} m(m-1)(m-2)P_m,$$

where M denotes the maximum number of mRNA molecules that a single cell can produce. By the law of large numbers, these converge to e_1, e_2, and e_3. Then, taking the relations $r_1 = \hat{e}_1$, $r_2 = \hat{e}_2/\hat{e}_1$, and $r_3 = \hat{e}_3/\hat{e}_2$ into Eq (2.3), we obtain the estimated parameters.

2.2.2. Maximum likelihood estimation

The maximum likelihood estimation seeks the parameter values that maximize the log-likelihood function [9, 11]

$$L(\theta) = \sum_m N(m) \log P_m(\theta),$$

where $\theta = (k_{on}, k_{off}, k_b)$ is the parameter set, $N(m)$ denotes the number of cells with m copies of mRNA, and $P_m(\theta)$ denotes the steady-state mRNA distribution with parameter set θ. The core of maximizing the log-likelihood function lies in the accurate computation or effective approximation of the steady-state mRNA probability distribution P_m. While the exact expression (2.2) for P_m involves confluent hypergeometric functions, direct computation is numerically intricate and computationally costly. Therefore, to enhance the feasibility and efficiency of likelihood function optimization, this paper considers four efficient and stable approximation methods in Section 2.3 of this paper.

2.2.3. Moment-reduced maximum likelihood estimation

Moment-reduced maximum likelihood estimation (MR-MLE) first utilizes the theoretical expressions of the mean E and fano factor ϕ (the ratio of the variance and the mean) in the telegraph model to derive analytical constraint relationships among the parameters. The mean E and fano factor ϕ are given by:

$$E = e_1 = \frac{k_{on}k_b}{k_{on} + k_{off}}, \quad \phi = \frac{e_2}{e_1} - e_1 + 1 = \frac{k_b(k_{on} + 1)}{k_{on} + k_{off} + 1} - \frac{k_{on}k_b}{k_{on} + k_{off}} + 1. \tag{2.4}$$

By solving the above equation, the switching rates k_{on} and k_{off} can be expressed as explicit functions of the synthesized rate k_b:

$$k_{on} = \frac{E(k_b + 1 - \phi - E)}{k_b(\phi - 1)}, \quad k_{off} = \frac{k_b - E}{E}k_{on}. \tag{2.5}$$

This step achieves an analytical dimensionality reduction from the three-dimensional parameter space (k_{on}, k_{off}, k_b) to the one-dimensional subspace of k_b. To ensure the biological plausibility of the estimated parameters, we examine the positivity conditions for k_{on} and k_{off}. It follows from Eqs (2.4) and (2.5) that $k_{on} > 0$ and $k_{off} > 0$ require $\phi > 1$ and $k_b > E$. It is important to note that the telegraph model itself theoretically satisfies $\phi \geq 1$, with $\phi = 1$ corresponding to the constitutive expression with $k_{off} = 0$.

On this basis, MR-MLE further constructs a log-likelihood function with respect to k_b:

$$L(k_b) = \sum_m N(m) \log \left(P_m(k_{on}(k_b), k_{off}(k_b), k_b)\right).$$

By maximizing this log-likelihood function, an estimate for k_b is obtained, and the corresponding estimates for k_{on} and k_{off} are simultaneously derived using Eq (2.5). This method preserves the statistical efficiency of maximum likelihood estimation while significantly reducing optimization complexity and enhancing the numerical stability and computational speed of parameter inference. The core of maximizing the log-likelihood function also lies in the accurate computation or effective approximation of the steady-state mRNA probability distribution P_m. The methods for approximating P_m are presented in detail in Section 2.3.

2.3. Methods for approximating P_m

2.3.1. Laplace approximation

The Laplace approximation to ${}_1F_1\left(k_{on} + m, k_{on} + k_{off} + m, -k_b\right)$ is given by [25]

$${}_1\hat{F}_1\left(k_{on} + m, k_{on} + k_{off} + m, -k_b\right) = (k_{on} + k_{off} + m)^{(k_{on}+k_{off}+m-1/2)} r^{-1/2} \left(\frac{y}{k_{on} + m}\right)^{k_{on}+m} \left(\frac{1-y}{k_{off}}\right)^{k_{off}} e^{-k_b y},$$

where

$$r = \frac{y^2}{k_{\text{on}} + m} + \frac{(1-y)^2}{k_{\text{off}}}, \quad y = \frac{2(k_{\text{on}} + m)}{k_{\text{on}} + k_{\text{off}} + k_{\text{b}} + m + \sqrt{(k_{\text{on}} + k_{\text{off}} + k_{\text{b}} + m))^2 - 4(k_{\text{on}} + m)k_{\text{b}}}}.$$

Substituting the above Laplace approximation into Eq (2.2) yields the Laplace-approximated form of the steady-state distribution P_m.

2.3.2. The finite state projection method

The CMEs given in Eq (2.1) can be expressed in vector form as $\frac{d}{dt}\mathbf{P}(t) = \mathbf{Q}(t)\mathbf{P}(t)$, or more specifically for the telegraph model,

$$\frac{d}{dt}\begin{pmatrix}\mathbf{P}_0(t)\\ \mathbf{P}_1(t)\\ \mathbf{P}_2(t)\\ \vdots\end{pmatrix} = \begin{pmatrix}\mathbf{A}(t)-\mathbf{T}(t) & \mathbf{D}(t) & 0 & \cdots\\ \mathbf{T}(t) & \mathbf{A}(t)-\mathbf{T}(t)-\mathbf{D}(t) & 2\mathbf{D}(t) & \ddots\\ 0 & \mathbf{T}(t) & \mathbf{A}(t)-\mathbf{T}(t)-2\mathbf{D}(t) & \ddots\\ \vdots & \ddots & \ddots & \ddots\end{pmatrix}\begin{pmatrix}\mathbf{P}_0(t)\\ \mathbf{P}_1(t)\\ \mathbf{P}_2(t)\\ \vdots\end{pmatrix}, \tag{2.6}$$

where the vector $\mathbf{P}_m(t) = (P_{0,m}(t), P_{1,m}(t))^T$ represents the probability of the two promoter states (gene *off* and *on*) at time t when exactly m mRNA molecules are present. In the expression above, the matrices governing promoter switching ($\mathbf{A}(t)$), transcription($\mathbf{T}(t)$), and degradation($\mathbf{D}(t)$) are given as:

$$\mathbf{A}(t) = \begin{pmatrix}-k_{\text{on}} & k_{\text{off}}\\ k_{\text{on}} & -k_{\text{off}}\end{pmatrix}, \quad \mathbf{T}(t) = \begin{pmatrix}0 & 0\\ 0 & k_{\text{b}}\end{pmatrix}, \quad \mathbf{D}(t) = \begin{pmatrix}1 & 0\\ 0 & 1\end{pmatrix}.$$

The state space of this system is infinite ($m = 0, 1, 2, \cdots$), directly solving Eq (2.6) is mathematically infeasible. To address this issue, we apply the finite state projection (FSP) method [26], which truncates the infinite-dimensional master equation to a finite-dimensional approximation while providing rigorous error bounds.

Let M_1 be the number of mRNA molecules such that the truncated portion of the vector $\mathbf{P}$ satisfies the specified error tolerance. Considering the steady-state scenario, Eq (2.6) reduces to

$$\begin{pmatrix}0\\ 0\\ \vdots\\ 0\\ 0\end{pmatrix} = \begin{pmatrix}\mathbf{A}-\mathbf{T} & \mathbf{D} & \cdots & 0 & 0\\ \mathbf{T} & \mathbf{A}-\mathbf{T}-\mathbf{D} & \cdots & 0 & 0\\ \vdots & \vdots & \ddots & \vdots & \vdots\\ 0 & 0 & \cdots & \mathbf{A}-\mathbf{T}-(M_1-1)\mathbf{D} & M_1\mathbf{D}\\ 0 & 0 & \cdots & \mathbf{T} & \mathbf{A}-\mathbf{T}-M_1\mathbf{D}\end{pmatrix}\begin{pmatrix}\mathbf{P}_0\\ \mathbf{P}_1\\ \vdots\\ \mathbf{P}_{M_1-1}\\ \mathbf{P}_{M_1}\end{pmatrix}, \tag{2.7}$$

where $\mathbf{P}_m = (P_{0,m}, P_{1,m})^T$ represents the steady-state probability vector for exactly m mRNA molecules, and

$$\mathbf{A} = \begin{pmatrix}-k_{\text{on}} & k_{\text{off}}\\ k_{\text{on}} & -k_{\text{off}}\end{pmatrix}, \quad \mathbf{T} = \begin{pmatrix}0 & 0\\ 0 & k_{\text{b}}\end{pmatrix}, \quad \mathbf{D} = \begin{pmatrix}1 & 0\\ 0 & 1\end{pmatrix}.$$

By adding a probability normalization constraint $\sum_{m=0}^{M_1}\mathbf{P}_m \approx 1$ as an additional row, Eq (2.7) can be further transformed into a solvable linear system:

$$\begin{pmatrix} 0 \\ 0 \\ \vdots \\ 0 \\ 1 \end{pmatrix} \approx \begin{pmatrix} \mathbf{A}-\mathbf{T} & \mathbf{D} & \cdots & 0 & 0 \\ \mathbf{T} & \mathbf{A}-\mathbf{T}-\mathbf{D} & \cdots & 0 & 0 \\ \vdots & \vdots & \ddots & \vdots & \vdots \\ 0 & 0 & \cdots & \mathbf{A}-\mathbf{T}-(M_1-1)\mathbf{D} & M_1\mathbf{D} \\ 0 & 0 & \cdots & \mathbf{T} & \mathbf{A}-\mathbf{T}-M_1\mathbf{D} \\ \mathbf{B} & \mathbf{B} & \cdots & \mathbf{B} & \mathbf{B} \end{pmatrix} \begin{pmatrix} \mathbf{P}_0 \\ \mathbf{P}_1 \\ \vdots \\ \mathbf{P}_{M_1-1} \\ \mathbf{P}_{M_1} \end{pmatrix}, \quad \mathbf{B} = \begin{pmatrix} 1 & 1 \end{pmatrix}.$$

The solution of this linear system provides a finite-dimensional approximation to the steady-state probability distribution P_m of the telegraph model, where $m \in [0, M_1]$. We have set $M_1 = 3M$, where M is the maximum number of mRNA molecules in experimental data.

2.3.3. Gauss–Jacobi quadrature

Here, we use the Gauss–Jacobi quadrature method to approximate the steady-state distribution P_m given in Eq (2.2). The integral representation for P_m (2.2) is given by

$$P_m = \frac{k_{\mathrm{b}}^m}{m!}\frac{\Gamma(k_{\mathrm{on}}+k_{\mathrm{off}})}{\Gamma(k_{\mathrm{off}})\Gamma(k_{\mathrm{on}})}\int_0^1 e^{-k_{\mathrm{b}}s}s^{k_{\mathrm{on}}+m-1}(1-s)^{k_{\mathrm{off}}-1}ds.$$

Let $s = (1+t)/2$, then the integral representation can be rewritten as

$$\begin{aligned} P_m &= \frac{k_{\mathrm{b}}^m}{m!}\frac{\Gamma(k_{\mathrm{on}}+k_{\mathrm{off}})}{\Gamma(k_{\mathrm{off}})\Gamma(k_{\mathrm{on}})}\left(\frac{1}{2}\right)^{k_{\mathrm{on}}+k_{\mathrm{off}}+m-1}\int_{-1}^1 e^{-k_{\mathrm{b}}(1+t)/2}(1+t)^{k_{\mathrm{on}}+m-1}(1-t)^{k_{\mathrm{off}}-1}dt \\ &= \frac{1}{B(k_{\mathrm{on}},k_{\mathrm{off}})}\frac{1}{2^{k_{\mathrm{on}}+k_{\mathrm{off}}-1}}\int_{-1}^1 \frac{e^{-k_{\mathrm{b}}(t+1)/2}}{m!}\left(\frac{k_{\mathrm{b}}(t+1)}{2}\right)^m(1+t)^{k_{\mathrm{on}}-1}(1-t)^{k_{\mathrm{off}}-1}dt, \end{aligned} \tag{2.8}$$

where $B(\cdot,\cdot)$ denotes the beta function. This expression coincides exactly with the standard formulation of the beta-Poisson distribution [11], and its integrand involves the characteristic structure of the Jacobi weight function

$$w^{\alpha,\beta}(t) = (1+t)^{\alpha}(1-t)^{\beta}, \quad \alpha = k_{\mathrm{on}}-1, \ \ \beta = k_{\mathrm{off}}-1.$$

The family of polynomials orthogonal on $[-1,1]$ with respect to the weight function $w^{\alpha,\beta}(t)$ are the Jacobi polynomials $J_n^{(\alpha,\beta)}(t)$, which admit the explicit Rodrigues-type representation

$$J_n^{(\alpha,\beta)}(t) = \frac{(-1)^n}{2^n n!(1+t)^{\alpha}(1-t)^{\beta}}\cdot\frac{d^n}{dt^n}\left[(1+t)^{\alpha+n}(1-t)^{\beta+n}\right], \ \ t\in[-1,1].$$

The roots of $J_n^{(\alpha,\beta)}(t)$, the quadrature nodes, can be obtained by solving an eigenvalue problem for a symmetric tridiagonal Jacobi matrix

$$\mathbf{J}_n = \begin{pmatrix} a_0 & b_0 & 0 & \cdots & 0 \\ b_0 & a_1 & b_1 & \cdots & 0 \\ 0 & b_1 & a_2 & \cdots & 0 \\ \vdots & \vdots & \vdots & \ddots & \vdots \\ 0 & 0 & 0 & \cdots & a_{n-1} \end{pmatrix},$$

where the diagonal and subdiagonal entries are defined for $k = 0, 1 \cdots, n-1$ as

$$a_k = \frac{\beta^2 - \alpha^2}{(2k+\alpha+\beta+2)(2k+\alpha+\beta)}, \quad b_k = \frac{2\sqrt{(k+1)(k+\alpha+1)(k+\beta+1)(k+\alpha+\beta+1)}}{(2k+\alpha+\beta+1)(2k+\alpha+\beta+2)}.$$

Let t_i, $i = 1, \cdots, n$, be the eigenvalues of $\mathbf{J}_n$which correspond precisely to the desired quadrature nodes. The associated quadrature weights are given by

$$w_i = \gamma_0 v_{i0}^2, \quad i = 1, \cdots, n,$$

where v_{i0} is the first component of the normalized eigenvector corresponding to the eigenvalue t_i, and

$$\gamma_0 = \int_{-1}^{1} (1+t)^\alpha (1-t)^\beta dt = \frac{2^{\alpha+\beta+1}\Gamma(\alpha+1)\Gamma(\beta+1)}{\Gamma(\alpha+\beta+2)}$$

is the zeroth moment (normalization constant) of the Jacobi weight function. Then the steady-state distribution P_m given in Eq (2.8) can be approximated by the Gauss–Jacobi quadrature method [27] as

$$P_m \approx \frac{1}{B(k_{\text{on}}, k_{\text{off}})} \frac{1}{2^{k_{\text{on}}+k_{\text{off}}-1}} \sum_{i=1}^{n} w_i \frac{e^{-k_{\text{b}}(t_i+1)/2}}{m!} \left(\frac{k_{\text{b}}(t_i+1)}{2}\right)^m.$$

2.4. Parameter estimation accuracy and consistency

Define the relative errors for the parameters k_{on}, k_{off} and k_{b} as:

$$RE_{k_{\text{on}}} = \frac{k_{\text{on}}^e - k_{\text{on}}^r}{k_{\text{on}}^r}, \quad RE_{k_{\text{off}}} = \frac{k_{\text{off}}^e - k_{\text{off}}^r}{k_{\text{off}}^r}, \quad RE_{k_{\text{b}}} = \frac{k_{\text{b}}^e - k_{\text{b}}^r}{k_{\text{b}}^r},$$

where the superscript e denotes the estimated value and r denotes the real value. If the absolute relative error of a parameter is less than 0.2, then we believe that it can reflect the realistic dynamic property of the telegraph model.

Define the modified mean relative error as

$$\text{MRE} = \frac{1}{S} \sum_{i=1}^{S} \frac{\left|par_i^1 - par_i^2\right|}{\max(par_i^1, par_i^2)},$$

where par_i^1 and par_i^2 denote the parameter estimates for the i-th gene obtained by two different methods, and S is the total number of gene groups in the dataset. This modified metric is symmetric, robust to outliers, and normalizes the results to the range [0,1] for straightforward comparison. It can thus be used to quantify the level of consistency between any two parameter estimation methods.

2.5. Datasets

The synthetic data of the telegraph model are generated by using the stochastic simulation algorithm (SSA) for $N = 10,000, 1000, 500, 100$ under 500 parameter sets. The parameter ranges are set as $k_{\text{on}} \in [0.01, 5]$, $k_{\text{off}} \in [0.01, 5]$, and $k_{\text{b}} \in [5, 50]$. The real experimental data were derived from 188 mouse embryonic stem (ES) cells with the C57 allele, covering a total of 6,169 genes, and 224 mouse fibroblasts with the C57 allele, covering a total of 6950 genes [9]. For these experimental data, we computed the empirical fano factor ϕ.

3. Results

3.1. Performance evaluation of methods on synthetic data

First, we evaluate the fitting performance of the nine parameter estimation methods by measuring the overall consistency between the actual and fitted distributions using the Hellinger distance (HD). As shown in Figures 1(a) and 2(a), the choice of parameter estimation method does not significantly affect the overall fit of the telegraph model to the synthetic data. This indicates that the model's fitting capability is largely independent of the inference algorithm used. However, good fitting performance does not directly reflect the accuracy of parameter estimation. Moreover, different parameter estimation methods vary significantly in terms of computational time. Therefore, in the following analysis, we will systematically evaluate the overall performance of these nine parameter estimation methods primarily from two dimensions: computational efficiency (fitting time) and parameter estimation accuracy.

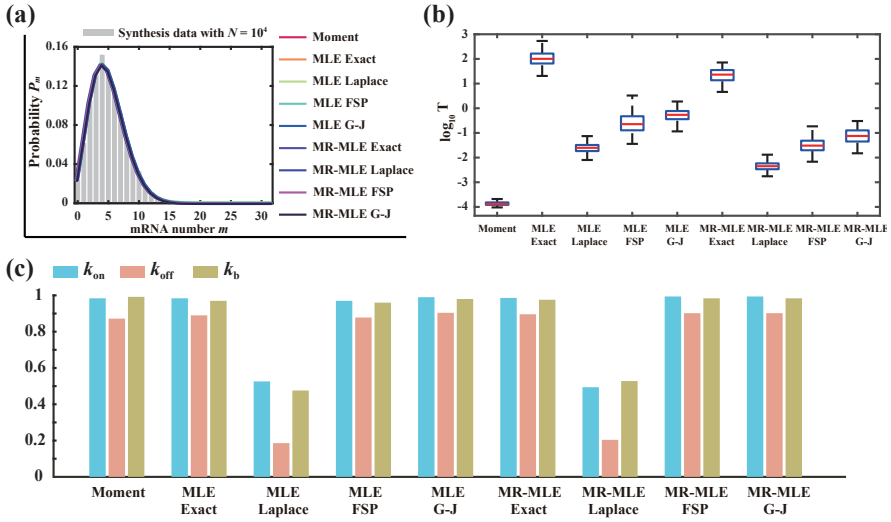

Figure 1. Comparison of nine parameter estimation methods based on the synthesis data with sample size $N = 10^4$. (a) All nine parameter estimation methods can effectively fit the steady-state distribution P_m of the synthesis data when the sample size N is sufficiently large. (b) Box plots of $\log_{10}$ T for the nine parameter estimation methods, where T denotes the fitting time. (c) For each of the nine parameter estimation methods, the empirical proportion of parameter sets satisfying $|RE_{k_{on}}| \leq 0.2$, $|RE_{k_{off}}| \leq 0.2$, and $|RE_{k_b}| \leq 0.2$ is computed.

We apply these nine parameter estimation methods to fit the synthetic data with sample size $N = 10^4$ and record both the estimated parameters and the corresponding fitting times. This sample size is sufficiently large to approximate the asymptotic steady-state distribution of the model, thereby providing a reliable benchmark for evaluating parameter inference methods under near-ideal sampling conditions. From the perspective of computational efficiency, the method of moments is by far the fastest, outperforming the other approaches by 4–6 orders of magnitude (Figure 1(b)). This is reasonable because the parameters estimated by the method of moments are given by explicit algebraic expressions (2.3) and can be computed directly without iterative optimization. Furthermore, for any fixed strategy for computing P_m, the fitting time required by the MR-MLE is consistently shorter than that of the MLE (Figure 1(b)). Using the exact confluent-hypergeometric expression for P_m yields

the lowest computational efficiency, as it involves costly numerical integration or series summation. (Figure 1(b)).

Figure 1(c) shows the empirical proportions of $|RE_{k_{on}}|$, $|RE_{k_{off}}|$, and $|RE_{k_b}|$ being less than 0.2. For all methods except those employing the Laplace approximation (MLE Laplace and MR-MLE Laplace), more than 95% of the parameter sets satisfy $|RE_{k_{on}}| \leq 0.2$, $|RE_{k_b}| \leq 0.2$; and approximately 90% of the parameter sets meet $|RE_{k_{off}}| \leq 0.2$. This indicates that, under sufficiently large sample sizes, the seven non-Laplace-based methods recover the true synthetic parameters with high reliability. In contrast, although the Laplace approximation reduces computational time (Figure 1(b)), it leads to strikingly poor parameter accuracy (Figure 1(c)). Thus, although computationally attractive, Laplace-based inference fails to deliver trustworthy kinetic estimates in this setting.

To investigate the influence of sample size on the results, we apply these nine parameter estimation methods to fit the synthetic data with sample sizes $N = 100, 500, 1000$, respectively. All nine methods maintain consistent fitting performance across different sample sizes (Figure 2(a)). Furthermore, the computational efficiency of the methods does not vary significantly with sample size (Figures 1(b) and 2(b)). Regardless of sample size, the parameter estimation accuracy of MLE Laplace and MR-MLE Laplace remains consistently poor (Figure 2(c)). In contrast, the remaining seven methods achieve comparable accuracy, though their performance systematically declines as the sample size decreases (Figure 2(c)).

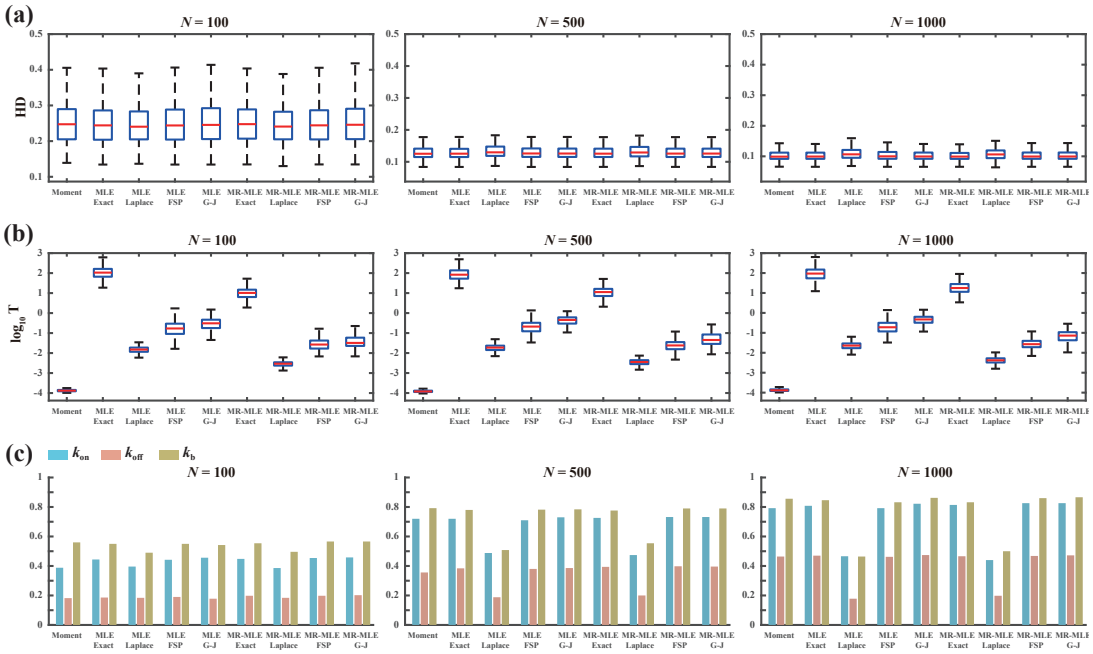

Figure 2. Comparison of nine parameter estimation methods based on the synthesis data with different sample sizes. (a) Box plots of Hellinger distances (HD) for the parameter estimation methods at sample size $N = 100, 500, 1000$. (b) Box plots of $\log_{10}$ T for the parameter estimation methods at sample size $N = 100, 500, 1000$, where T denotes the fitting time. (c) For each of the nine parameter estimation methods, the empirical proportion of parameter sets satisfying $|RE_{k_{on}}| \leq 0.2$, $|RE_{k_{off}}| \leq 0.2$, or $|RE_{k_b}| \leq 0.2$ is computed with sample size $N = 100, 500, 1000$.

When $N = 100$, the estimation accuracy for all three parameters is notably poor. This indicates that under small sample conditions, the estimated parameters are unlikely to reflect the true parameters. When $N \geq 500$, the accuracy rates for k_{on} and k_{b} exceed 70%, suggesting that the estimated k_{on} and k_{b} can adequately capture the true parameters at this scale. However, even with larger sample sizes, the accuracy of k_{off} remains below 50%, implying that this parameter is difficult to estimate stably and accurately within the current inference framework, and its estimates exhibit significant systematic bias. In summary, under limited sample sizes, the estimated k_{off} struggles to accurately reflect its real kinetic properties, thereby failing to meet the quantitative precision requirements for inactivation rate in subsequent biological analyses.

For synthetic data, balancing computational efficiency with estimation accuracy, the method of moments performs best, followed by MR-MLE FSP and MR-MLE G-J. Nevertheless, the theoretical justification of the method of moments rests on Gaussian-like distributional assumptions, whereas real single-cell data often exhibit highly asymmetric or over-dispersed distributions due to low copy numbers of biochemical molecules such as DNA, RNA, or protein [2, 9, 31]. Consequently, the applicability of the method of moments may be limited in experimental data.

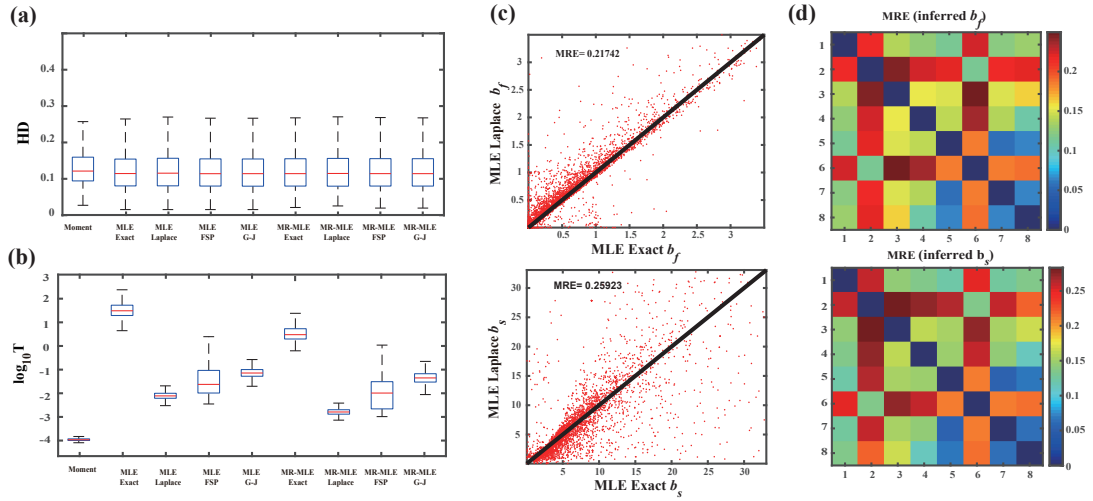

Figure 3. Comparison of parameter estimation methods based on experiment Data (ES cells). (a) Box plots of Hellinger distances (HD) for the nine parameter estimation methods . (b) Box plots of $\log_{10}$ T for the nine parameter estimation methods, where T denotes the fitting time. (c) Scatter plots compare the relationship between the burst parameters estimated by MLE Exact and those estimated by MLE Laplace using mouse ES cells data. The MRE indicates the level of consistency between the two methods. The symbols b_f and b_s denote the burst frequency and burst size, respectively. (d) Numbers 1–8 denote parameter inference methods: MLE Exact, MLE Laplace, MLE FSP, MLE G-J, MR-MLE Exact, MR-MLE Laplace, MR-MLE FSP, and MR-MLE G-J. The heatmap illustrates the pairwise MRE of estimation results among the eight methods. MLE Laplace or MR-MLE Laplace exhibit significantly higher MRE with respect to the other six methods than the intermethod MRE of the remaining methods.

3.2. Performance evaluation of methods on experiment data

In this section, we systematically compare the performance of the nine parameter estimation methods introduced earlier, based on real experimental data with ES cells and fibroblasts [9]. All nine methods continue to show consistent fitting performance (Figures 3(a) and A1(a)). Furthermore, the HD calculated from the experimental data closely matches those obtained from the synthetic data, and the computational efficiency of the nine parameter estimation methods remains consistent across both data types (Figures 3(b) and A1(b)). These results indicate that the performance of methods validated on synthetic data can be reasonably extrapolated to real experiment data.

Although the method of moments offers high computational efficiency, its estimates are unstable under limited sample sizes, yielding unphysical negative parameter estimates for approximately 25% of the genes. This result does not imply a lack of biological significance for these genes. On the contrary, it may indicate that their expression patterns are highly dynamic or reside in critical regulatory states. In contrast, for genes within the telegraph model's scope of applicability, both MLE and MR-MLE produced strictly positive parameter estimates. In our tests, 99% of genes satisfied this condition ($\phi > 1$). For these genes, no negative estimates were observed under either likelihood-based method. Given these limitations, we exclude the method of moments from further analysis and proceed to compare the remaining eight methods with real experimental data.

Practical biological analyses often focus on two key kinetic characteristics: burst frequency (a measure of the average rate at which transcription switches from an inactive state to an active state) and burst size (representing the average number of mRNA molecules generated by a gene during each active period) [4, 9]. By fitting the data with the telegraph model, we derived two effective parameters: the burst frequency $b_f = k_{\text{on}}$ and the burst size $b_s = k_{\text{b}}/k_{\text{off}}$. Unlike simulated data, the true kinetic parameters corresponding to experimental data are unknown and cannot be directly observed. To this end, we systematically compared the burst parameters in a pairwise manner using the modified mean relative error to evaluate the consistency between different methods. Specifically, we calculated the deviation of each data point from the 1:1 reference line and quantified this deviation using the MRE of all data points, thereby assessing the consistency of the parameter inference results between the two methods (Figures 3(c) and A1(c)).

Figures 3(d) and A1(d) show that the parameter estimates obtained by the MLE Laplace or MR-MLE Laplace methods exhibit the weakest consistency with those from the other methods, which is reflected by their significantly higher MRE. Combined with the aforementioned conclusion from synthetic data analysis, that is, MLE Laplace and MR-MLE Laplace fail to accurately reflect the real parameters, whereas the other methods demonstrate good parameter recovery. Therefore, we reasonably conclude that MLE Laplace and MR-MLE Laplace are unlikely to provide reliable kinetic estimates when fitting real experimental data.

In contrast, the MRE among the parameter values estimated by the other six methods was small, indicating consistent inference results across different computational strategies (Figures 3(d) and A1(d)). Among these six parameter estimation methods, MR-MLE FSP and MR-MLE G-J demonstrate the highest computational efficiency.

For the FSP method, the state space is truncated at $M_1 = 3M$, where M is the largest observed mRNA count for the gene. Consequently, for highly expressed genes or those with high expression variability, the steady-state distribution often exhibits a pronounced long-tail behavior, leading to a substantially larger truncation bound M_1. This results in a sharp expansion of the state-space

dimension, which in turn significantly increases the fitting time. This mechanism explains the greater variability in fitting times observed for the FSP method in Figures 3(b) and A1(b). Hence, considering both computational speed and inferential reliability, we recommend MR-MLE G-J as the preferred choice for fitting real single-cell gene-expression data.

4. Conclusions

In this paper, we systematically compare three parameter estimation frameworks (the method of moments, MLE, and MR-MLE), each combined with four computational strategies for the steady-state mRNA distribution P_m (exact confluent hypergeometric solution, Laplace approximation, FSP, and Gauss–Jacobi quadrature). This yields a total of nine distinct parameter estimation methods, which are evaluated along two key dimensions: computational efficiency and parameter estimation accuracy. Evaluation of the goodness of fit using HD reveals that, under the same sample size, the HD values obtained by the nine methods are largely consistent. However, HD increases as the sample size decreases. The HD for experimental data with 188 samples falls between the HD values obtained from synthetic data with 100 and 500 samples, illustrating a smooth transition of the methods from simulation to real-world application.

Under the same sample size, the parameter estimation accuracy of the three inference frameworks remains largely consistent. However, their accuracy systematically declines as the sample size decreases. Notably, none of the methods reliably recover the true inactivation rate k_{off}; under limited sample sizes, but both the activation rate k_{on} and synthesized rate k_{b} are estimated accurately when the sample size $N \geq 500$. This may be attributed to the structural characteristics of the telegraph model itself. In the sensitivity analysis of the three parameters with respect to the fano factor, the parameter k_{off} exhibits the lowest sensitivity (Figure A2), resulting in its poorest identifiability. Therefore, subsequent biological interpretations should focus on the burst frequency (k_{on}) and burst size ($k_{\text{b}}/k_{\text{off}}$) [9], rather than discussing k_{off} in isolation.

The computational efficiency of each method remains stable across different data sources (synthetic and experimental data) and varying sample sizes. Among three inference frameworks, the method of moments achieves the highest computational efficiency, and the MR-MLE we propose improves the computational efficiency of classical MLE. However, when the method of moments is fitted to experimental data, about 25% of genes yield negative parameter estimates, whereas MLE and MR-MLE do not exhibit such problems (Figure A3). Nevertheless, approximately 1% of genes showed $\phi \leq 1$, which may correspond to more complex regulatory mechanisms [32]. This outcome primarily stems from random fluctuations in sample moments under small-sample conditions. With limited sample sizes, estimates of the sample mean and variance may violate the inherent constraints of the theoretical moments in the telegraph model, leading to parameter solutions that fall outside the feasible range. Consequently, using the method of moments for experimental data fitting would lead to the exclusion of a considerable proportion of genes. Among these excluded genes, many may exhibit highly dynamic expression patterns or reside in critical regulatory states, implying biological relevance. Therefore, although computationally very fast, the method of moments is not well-suited for experimental data analysis. Introducing moment constraints may exacerbate the bias caused by fluctuations in the sample moments. However, this effect was not pronounced in our experiments, as the estimation accuracy of MLE and MR-MLE was nearly identical. Under ideal large-sample

conditions, MR-MLE is asymptotically equivalent to the full parametric MLE, which is also supported by the observation that the estimation accuracy of MLE and MR-MLE was similar across all sample sizes (Figures 1(c) and 2(c)).

We therefore conclude that MR-MLE is a more practical choice for estimating kinetic parameters. As the implementation of MR-MLE relies on the computation of the steady-state distribution P_m, we next examine the impact of four different methods for calculating P_m on the performance of MR-MLE. The study reveals that using the exact expression for P_m results in the lowest computational efficiency. Although the Laplace approximation improves computational speed, its estimated parameters fail to accurately reflect the true kinetic values. For the synthesis data, the FSP method and the Gauss–Jacobi quadrature method perform comparably in terms of computational efficiency and parameter estimation accuracy. However, for experimental data, the computational efficiency of the FSP method shows considerable variability, whereas the Gauss–Jacobi method remains stable. This is because the state-space truncation in FSP depends on the observed maximum mRNA count. In contrast, the computational cost of the Gauss–Jacobi quadrature depends only on the predefined number of quadrature nodes and is independent of gene expression levels.

Therefore, supported by Gauss–Jacobi quadrature, MR-MLE G-J achieves both high computational efficiency and robust parameter inference in real gene expression data, making it our final recommended method. While the steady-state assumption enables tractable parameter inference, it inherently limits our ability to capture the temporal dynamics of gene expression during critical biological processes such as development, differentiation, or disease progression. Future work should therefore focus on developing and optimizing inference frameworks that explicitly account for time-varying kinetics [32, 33], enabling the quantification of transient expression dynamics from time-resolved single-cell data.

Code accessibility

MATLAB code implementing nine methods of parameter inference can be accessed via the https://github.com/LChen-hcy/parameter-inference.

Use of AI tools declaration

The authors declare they have not used Artificial Intelligence (AI) tools in the creation of this article.

Acknowledgments

Liang Chen was supported by the Innovation Research Grant No. JCCX2024-014 for Postgraduate of Guangzhou University. Ying Sheng was supported by the Innovation Research Grant No. JCCX2025017 for Postgraduate of Guangzhou University. Feng Jiao was supported by the Natural Science Foundation of China No. 12271118.

Conflict of interest

Feng Jiao is a Guest Editor of special issue "Applied Dynamical Systems and Mathematical Biology" for Electronic Research Archive. He was not involved in the editorial review and the decision to publish this article. The authors declare there are no conflicts of interest.

Appendix

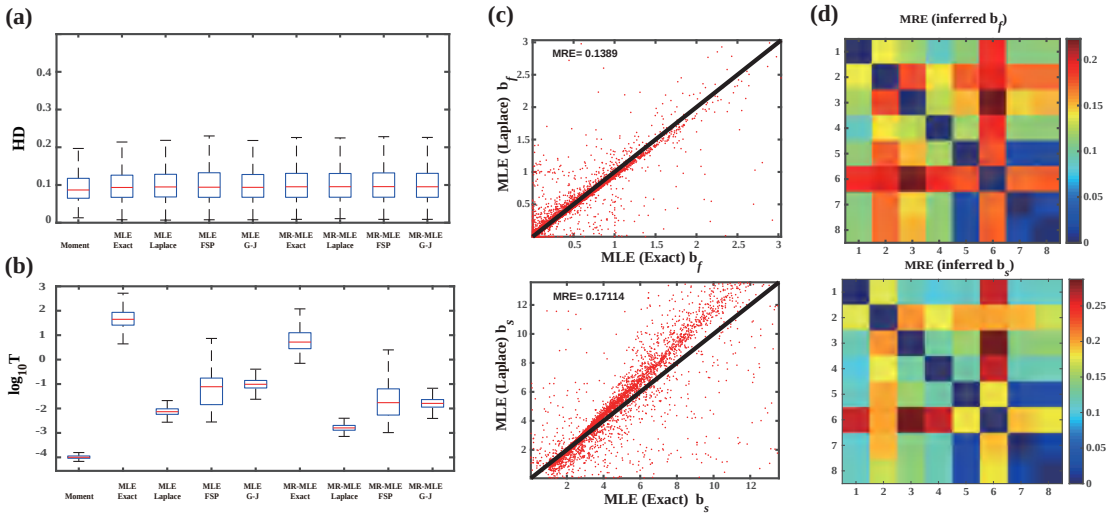

Figure A1. Comparison of parameter estimation methods based on experiment data (mouse fibroblast cells). (a) Box plots of Hellinger distances (HD) for the parameter estimation methods . (b) Box plots of $\log_{10}$ T for the parameter estimation methods, where T denotes the fitting time. (c) Scatter plots compare the relationship between the burst parameters estimated by MLE Exact and those estimated by MLE Laplace using mouse ES cells data. The MRE indicates the level of consistency between the two methods. The symbols b_f and b_s denote the burst frequency and burst size, respectively. (d) Numbers 1–8 denote parameter inference methods: MLE Exact, MLE Laplace, MLE FSP, MLE G-J, MR-MLE Exact, MR-MLE Laplace, MR-MLE FSP, and MR-MLE G-J. The heatmap illustrates the pairwise MRE of estimation results among the eight methods. MLE Laplace or MR-MLE Laplace exhibit significantly higher MRE with respect to the other six methods than the MRE of the remaining methods.

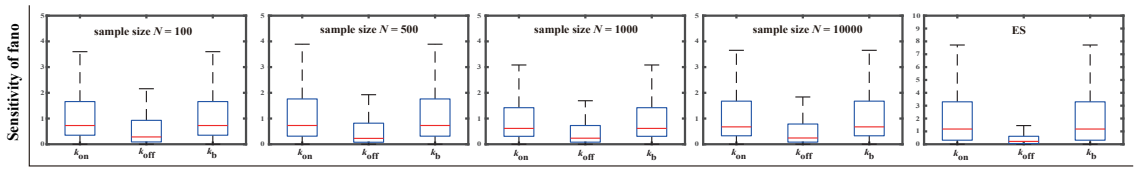

Figure A2. Sensitivity analysis of fano factor with respect to parameters. After estimating the parameters based on synthetic and experimental data (ES cells), we computed the sensitivity of the fano factor derived from the telegraph model with respect to the three parameters. The results show that the parameter k_{off} exhibits the lowest sensitivity.

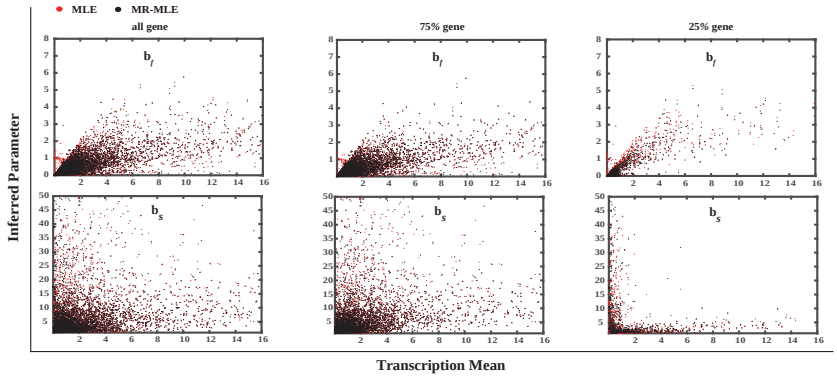

Figure A3. Burst parameters inferred by MLE and MR-MLE based on embryonic stem cells. All genes refer to all genes in embryonic stem cells. The 75% gene subset represents the genes after removing those with negative parameter values inferred by the method of moments. The 25% gene subset represents the genes with negative parameter values inferred by the method of moments. The scatter plot shows the variation of b_f and b_s with the transcription mean.

References

1. M. Kærn, T. C. Elston, W. J. Blake, J. J. Collins, Stochasticity in gene expression: from theories to phenotypes, *Nat. Rev. Genet.*, **6** (2005), 451–464. https://doi.org/10.1038/nrg1615
2. I. Golding, J. Paulsson, S. M. Zawilski, E. C. Cox, Real-time kinetics of gene activity in individual bacteria, *Cell*, **123** (2005), 1025–1036. https://doi.org/10.1016/j.cell.2005.09.031
3. T. L. Lenstra, J. Rodriguez, H. Chen, D. R. Larson, Transcription dynamics in living cells, *Annu. Rev. Biophys.*, **45** (2016), 25–47. https://doi.org/10.1146/annurev-biophys-062215-010838
4. D. B. Mahat, N. D. Tippens, J. D. Martin-Rufino, S. K. Waterton, J. Fu, S. E. Blatt, et al., Single-cell nascent RNA sequencing unveils coordinated global transcription, *Nature*, **631** (2024), 216–223. https://doi.org/10.1038/s41586-024-07517-7
5. A. Raj, C. S. Peskin, D. Tranchina, D. Y. Vargas, S. Tyagi, Stochastic mrna synthesis in mammalian cells, *PLoS Biol.*, **4** (2006), e309. https://doi.org/10.1371/journal.pbio.0040309

6. L. H. So, A. Ghosh, C. Zong, L. A. Sepúlveda, R. Segev, I. Golding, General properties of transcriptional time series in Escherichia coli, *Nat. Genet.*, **43** (2011), 554–560. https://doi.org/10.1038/ng.821
7. J. K. Kim, J. C. Marioni, Inferring the kinetics of stochastic gene expression from single-cell RNA-sequencing data, *Genome Biol.*, **14** (2013), R7. https://doi.org/10.1186/gb-2013-14-1-r7
8. L. Chen, C. Zhu, F. Jiao, A generalized moment-based method for estimating parameters of stochastic gene transcription, *Math. Biosci.*, **345** (2022), 108780. https://doi.org/10.1016/j.mbs.2022.108780
9. A. J. Larsson, P. Johnsson, M. Hagemann-Jensen, L. Hartmanis, O. R. Faridani, B. Reinius, et al., Genomic encoding of transcriptional burst kinetics, *Nature*, **565** (2019), 251–254. https://doi.org/10.1038/s41586-018-0836-1
10. S. S. Dey, J. E. Foley, P. Limsirichai, D. V. Schaffer, A. P. Arkin, Orthogonal control of expression mean and variance by epigenetic features at different genomic loci, *Mol. Syst. Biol.*, **11** (2015), MSB145704. https://doi.org/10.15252/msb.20145704
11. T. N. Vu, Q. F. Wills, K. R. Kalari, N. Niu, L. Wang, M. Rantalainen, et al., Beta-Poisson model for single-cell RNA-seq data analyses, *Bioinformatics*, **32** (2016), 2128–2135. https://doi.org/10.1093/bioinformatics/btw202
12. L. B. Carey, D. van Dijk, P. M. Sloot, J. A. Kaandorp, E. Segal, Promoter sequence determines the relationship between expression level and noise, *PLoS Biol.*, **11** (2013), e1001528. https://doi.org/10.1371/journal.pbio.1001528
13. D. L. Jones, R. C. Brewster, R. Phillips, Promoter architecture dictates cell-to-cell variability in gene expression, *Science*, **346** (2014), 1533–1536. https://doi.org/10.1126/science.1255301
14. C. Zong, L. H. So, L. A. Sepúlveda, S. O. Skinner, I. Golding, Lysogen stability is determined by the frequency of activity bursts from the fate-determining gene, *Mol. Syst. Biol.*, **6** (2010), MSB201096. https://doi.org/10.1038/msb.2010.96
15. F. Jiao, M. Tang, Quantification of transcription noise's impact on cell fate commitment with digital resolutions, *Bioinformatics*, **38** (2022), 3062–3069. https://doi.org/10.1093/bioinformatics/btac277
16. T. I. Lee, R. A. Young, Transcriptional regulation and its misregulation in disease, *Cell*, **152** (2013), 1237–1251. https://doi.org/10.1016/j.cell.2013.02.014
17. R. D. Dar, N. N. Hosmane, M. R. Arkin, R. F. Siliciano, L. S. Weinberger, Screening for noise in gene expression identifies drug synergies, *Science*, **344** (2014), 1392–1396. https://doi.org/10.1126/science.1250220
18. E. Shapiro, T. Biezuner, S. Linnarsson, Single-cell sequencing-based technologies will revolutionize whole-organism science, *Nat. Rev. Genet.*, **14** (2013), 618–630. https://doi.org/10.1038/nrg3542
19. A. Mortazavi, B. A. Williams, K. McCue, L. Schaeffer, B. Wold, Mapping and quantifying mammalian transcriptomes by RNA-Seq, *Nat. Methods*, **5** (2008), 621–628. https://doi.org/10.1038/nmeth.1226

20. J. R. Moffitt, J. Hao, G. Wang, K. H. Chen, H. P. Babcock, X. Zhuang, High-throughput single-cell gene-expression profiling with multiplexed error-robust fluorescence in situ hybridization, *Proc. Natl. Acad. Sci. U.S.A.*, **113** (2016), 11046–11051. https://doi.org/10.1073/pnas.1612826113
21. F. Jiao, J. Li, T. Liu, Y. Zhu, W. Che, L. Bleris, et al., What can we learn when fitting a simple telegraph model to a complex gene expression model?, *PLoS Comput. Biol.*, **20** (2024), e1012118. https://doi.org/10.1371/journal.pcbi.1012118
22. S. Y. Kim, D. Huh, Z. Zhou, E. Y. Mun, A comparison of Bayesian to maximum likelihood estimation for latent growth models in the presence of a binary outcome, *Int. J. Behav. Dev.*, **44** (2020), 447–457. https://doi.org/10.1177/0165025419894730
23. P. Thomas, V. Shahrezaei, Coordination of gene expression noise with cell size: analytical results for agent-based models of growing cell populations, *J. R. Soc. Interface*, **18** (2021), 20210274. https://doi.org/10.1098/rsif.2021.0274
24. S. Iyer-Biswas, F. Hayot, C. Jayaprakash, Stochasticity of gene products from transcriptional pulsing, *Phys. Rev. E*, **79** (2009), 031911. https://doi.org/10.1103/PhysRevE.79.031911
25. R. W. Butler, A. T. Wood, Laplace approximations for hypergeometric functions with Hermitian matrix argument, *Ann. Stat.*, **30** (2002), 1155–1177. Available from: https://www.jstor.org/stable/1558699.
26. B. Munsky, M. Khammash, The finite state projection algorithm for the solution of the chemical master equation, *J. Chem. Phys.*, **124** (2006), 044104. https://doi.org/10.1063/1.2145882
27. F. B. Hildebrand, *Introduction to Numerical Analysis*, New York: Dover Publications, 1987.
28. J. Paulsson, M. Ehrenberg, Noise in a minimal regulatory network: plasmid copy number control, *Q. Rev. Biophys.*, **34** (2001), 1–59. https://doi.org/10.1017/S0033583501003663
29. C. Jia, R. Grima, Coupling gene expression dynamics to cell size dynamics and cell cycle events: Exact and approximate solutions of the extended telegraph model, *iScience*, **26** (2023), 105746. https://doi.org/10.1016/j.isci.2022.105746
30. J. Peccoud, B. Ycart, Markovian modeling of gene-product synthesis, *Theor. Popul Biol.*, **48** (1995), 222–234. https://doi.org/10.1006/tpbi.1995.1027
31. B. Munsky, G. Li, Z. R. Fox, D. P. Shepherd, G. Neuert, Distribution shapes govern the discovery of predictive models for gene regulation, *Proc. Natl. Acad. Sci. U.S.A.*, **115** (2018), 7533–7538. https://doi.org/10.1073/pnas.1804060115
32. C. Zhu, L. Chen, Z. Qiu, J. Chen, F. Jiao, J. Yu, Correlation and distinction between stochastic gene transcription models with and without polymerase dynamics, *Phys. Rev. Res.*, **7** (2025), 023050. https://doi.org/10.1103/PhysRevResearch.7.023050
33. K. Wen, Y. Liao, J. Wang, S. Choubey, F. Jiao, A moments-based approach for inferring mechanisms of transcriptional regulation using nascent RNA data, *Biophys. J.*, **125** (2026), 1257–1275. https://doi.org/10.1016/j.bpj.2026.01.030

AIMS Press